International Journal of Engineering and Science Invention (IJESI)
ISSN (Online): 2319-6734, ISSN (Print): 2319-6726
www.ijesi.org ||Volume 14 Issue 8 August 2025 || PP 04-13

Phase Behavior and Thermodynamic Insights into Cholinium-Based Magnetic Ionic Liquid Aqueous Two-Phase Systems

Dr. Sunil Kumar MIshra
Assistant Professor,
Department of Chemistry D. A-V. College, Kanpur

Dr. Udai Pratap Singh
(Corresponding author) Assistant Professor,
Department of Chemistry D. A-V. College, Kanpur

Abstract: *This study investigates the phase behavior and thermodynamics of aqueous two-phase systems (ATPSs) formed with cholinium-based magnetic ionic liquids (MILs). Three MILs were synthesized and characterized, demonstrating their efficacy in forming magnetically responsive ATPSs for advanced separation applications. Phase diagrams were determined for MIL-ATPSs [N_{11n}(2OH)][TEMPO-OSO_3] (with varying alkyl chain lengths), salts, and water across different temperatures. Binodal data were accurately fitted using the Merchuk equation. Results reveal that MIL structure, temperature, and salt type profoundly affect phase behavior. Structural features and viscosity of the MILs significantly influence phase formation. The salting-out effect emerged as the key driving force, correlating with salt hydration thermodynamics ($\Delta_{hyd}G$ and $\Delta_{hyd}S$). These findings provide valuable experimental and theoretical insights to advance responsive separation technologies.*

Keywords: *Aqueous Two-Phase Systems (ATPSs), Magnetic Ionic Liquids (MILs), Cholinium-based ILs, MerchukEquation, Salting-out Effect*

I. INTRODUCTION:

Aqueous two-phase systems (ATPSs) offer an environmentally friendly and efficient platform for diverse separation and purification applications, including biomolecules and pharmaceuticals [1, 2]. The integration of ionic liquids (ILs) into ATPSs has significantly expanded their versatility due to ILs' unique physicochemical properties and tunability [3]. A groundbreaking advancement in this field is the emergence of magnetic ionic liquids (MILs), which enable ATPSs to become magnetically responsive [4]. This magnetic functionality facilitates swift and efficient phase separation via external magnetic fields, greatly simplifying downstream recovery processes compared to conventional methods [5]. While the promise of MIL-ATPSs for advanced extraction is evident, a comprehensive understanding of their fundamental phase behavior and underlying thermodynamic principles, particularly for novel cholinium-based MILs, is crucial for their rational design and broader implementation. This study systematically investigates the phase behavior of cholinium-based MIL-ATPSs, exploring the influences of MIL structure, temperature, and salt type, while providing detailed thermodynamic insights to catalyze further advancements in responsive separation science.

II. Experimental Section

2.1. Materials & Apparatus

All chemical reagents, including precursors for magnetic ionic liquid (MIL) synthesis (e.g., choline hydroxide, 4-OH-TEMPO, chlorosulfonic acid) and analytical-grade salts, were obtained from commercial suppliers (e.g., Titan Technology Co., Ltd., InnoChem Technology Co., Ltd.) with ≥98% purity. Ultrapure water was generated using an ultra-pure water system. MIL synthesis and purification details are provided in the Supporting Information.

Key instrumentation for material characterization and experimental control included: an electronic analytical balance (Sartorius, ±0.1 mg); a mass spectrometer (Waters ZQ2000, ESI source) for MS data; a vibration sample magnetometer (Quantum Design MPMS SQUID) for magnetic properties; an FT-IR Spectrometer (PerkinElmer Spectrum Two); a UV–VIS spectrophotometer (Shimadzu UV-1900i); and a thermogravimetric analyzer (NETZSCH STA449F3). Temperature for all experimental systems was precisely controlled by a low-temperature thermostat (Hengping, ±0.05 K).

2.2. Viscosity Measurement

The viscosity of the three synthesized MILs was measured across a temperature range of 283.15 K to 323.15 K (5 K intervals) using the capillary method. A calibrated viscometer (4 mm diameter, using glycerol as standard) was employed within a thermostatic water bath (±0.05 K). Viscosity (η) was calculated based on the flow time (t), density (ρ), and viscometer constant (c): $\eta = \rho \times c \times t$. The experimental viscosity data were subsequently fitted using the Vogel–Fulcher–Tamman (VFT), Litovitz, and Arrhenius equations to analyze temperature dependency.

2.4. Phase Diagrams and Tie Lines

The binodal curves for the MIL-ATPSs with various salts were determined using the cloud point titration method [6]. This involved titrating a known amount of MIL solution with salt solution until turbidity appeared, then adding water to achieve clarity, and repeating the process to map the phase boundary. All titrations were performed in a jacketed glass vessel under constant stirring. The experimental binodal data were then accurately correlated using the empirical Merchuk equation [7].

To determine the tie lines, ternary mixtures of known composition were prepared within the two-phase region. These mixtures were rigorously stirred in a jacketed glass vessel to ensure equilibrium. Subsequently, the top and bottom phases were carefully separated, and their compositions were determined. From these compositions, the tie-line length (TLL) and the slope (S) of the tie-lines were calculated using established equations [7].

III. Results And Discussion

3.1.1. Magnetization

The magnetic properties of the synthesized MILs originate from the single electron structure of the NO˙ radical in the [TEMPO-OSO_3]- anion, which is crucial for magnet-assisted phase separation. Magnetization curves were investigated as a function of applied magnetic field (±20,000 Oe) at 298 K. All MILs exhibited S-shaped hysteresis loops, indicative of typical paramagnetic behavior. This demonstrates that the MILs align with an external magnetic field but show disordered arrangement in its absence. Notably, [N_{114}(2OH)][TEMPO-OSO_3] showed the strongest magnetic susceptibility, reaching 63 emu/mol. These findings confirm the MILs' responsiveness to an applied magnetic field, making them suitable for practical applications.

3.1.2. FT-IR Spectra

FT-IR spectroscopy was performed to characterize the synthesized MILs and confirm their chemical structures. Analysis of the spectra revealed characteristic absorption peaks consistent with the expected functional groups. Specifically, peaks above 3000 cm^{-1} were attributed to O–H stretching vibrations from the cationic structure. Saturated C–H stretching vibrations (methyl and methylene) were observed between 2800 cm^{-1} and 3000 cm^{-1}. Vibrations related to the anion included a peak at 1715 cm^{-1} (skeleton vibration), C–H asymmetric bending at 1466 cm^{-1}, and symmetric in-plane C–H bending (gem-dimethyl) at 1379 cm^{-1} and 1364 cm^{-1}. Furthermore, a band at 1215 cm^{-1} was assigned to C–N stretching, while N–O stretching in the anion appeared at 1061 cm^{-1}. Asymmetric and symmetric O–S–O stretching vibrations in the anion were also identified at 982 cm^{-1} and 860 cm^{-1}, respectively. These spectral features collectively confirmed the successful synthesis and structural integrity of the cholinium-based MILs.

3.1.3. UV–Visible Spectra

UV–visible absorption spectroscopy was conducted on the cholinium-based MILs across a wavelength range of 200–700 nm. The primary UV absorption in these MILs is attributed to their anionic structure. All three MILs exhibited a maximum absorption wavelength (λ_{max}) consistently around 245 nm. Minor variations in λ_{max} were observed, which are likely influenced by the differing cationic structures of the MILs.

3.1.4. TGA-DTG Analysis

Thermogravimetric Analysis (TGA) coupled with Derivative Thermogravimetry (DTG) was employed to assess the thermal stability of the magnetic ionic liquids (MILs). Given the structural similarity among the three MILs, the thermal behavior of [N_{112}(2OH)][TEMPO-OSO_3] served as a representative example. Samples were heated from 30 °C to 600 °C at a rate of 10 °C/min, revealing a four-step decomposition process. The initial weight loss (12.84%) below 230 °C was attributed to water desorption. A more significant weight loss (59.14%) occurred between 230 °C and 308 °C, peaking at 282.54 °C, corresponding to the breakdown of the organic group. Further weight loss was observed as the temperature increased, with the final stage (356 °C to 600 °C) linked to the removal of the –OH group.

3.1.5. ESI-MS Analysis

Electrospray Ionization Mass Spectrometry (ESI-MS) was utilized to confirm the precise structures and purity of the synthesized magnetic ionic liquids (MILs). All MILs consistently displayed a characteristic ionic peak at *m/z* 251, corresponding to the $[C_9H_{17}NO_5S]$- anion. Additionally, distinct ionic peaks were observed at *m/z* 118.16, 132.20, and 146.24, which successively matched the molecular weights of the respective cholinium-based cations. These results definitively confirm the anionic and cationic structures of the MILs.

3.2. Viscosity Analysis

The viscosity data for the three MILs were experimentally measured at various temperatures and are presented in Table 1. As shown in Fig. 1(a), the viscosity exhibited an exponential dependence on temperature. A clear trend emerged where viscosity increased with the elongation of the cationic chain, following the order: $[N_{114}(2OH)][TEMPO\text{-}OSO_3]$ >$[N_{113}(2OH)][TEMPO\text{-}OSO_3]$ >$[N_{112}(2OH)][TEMPO\text{-}OSO_3]$ [8-10]. This observation is attributed to stronger hydrogen bonding between the cation and anion as the cationic chain lengthens, leading to higher viscosity. Conversely, increasing temperature significantly reduced viscosity, likely due to a decrease in interparticle forces. Furthermore, a linear relationship was observed between lnη and 1/T (Fig. 1(b)), with a strong linear correlation coefficient (R^2) greater than 0.99; the corresponding fitting parameters are detailed in Table 2.

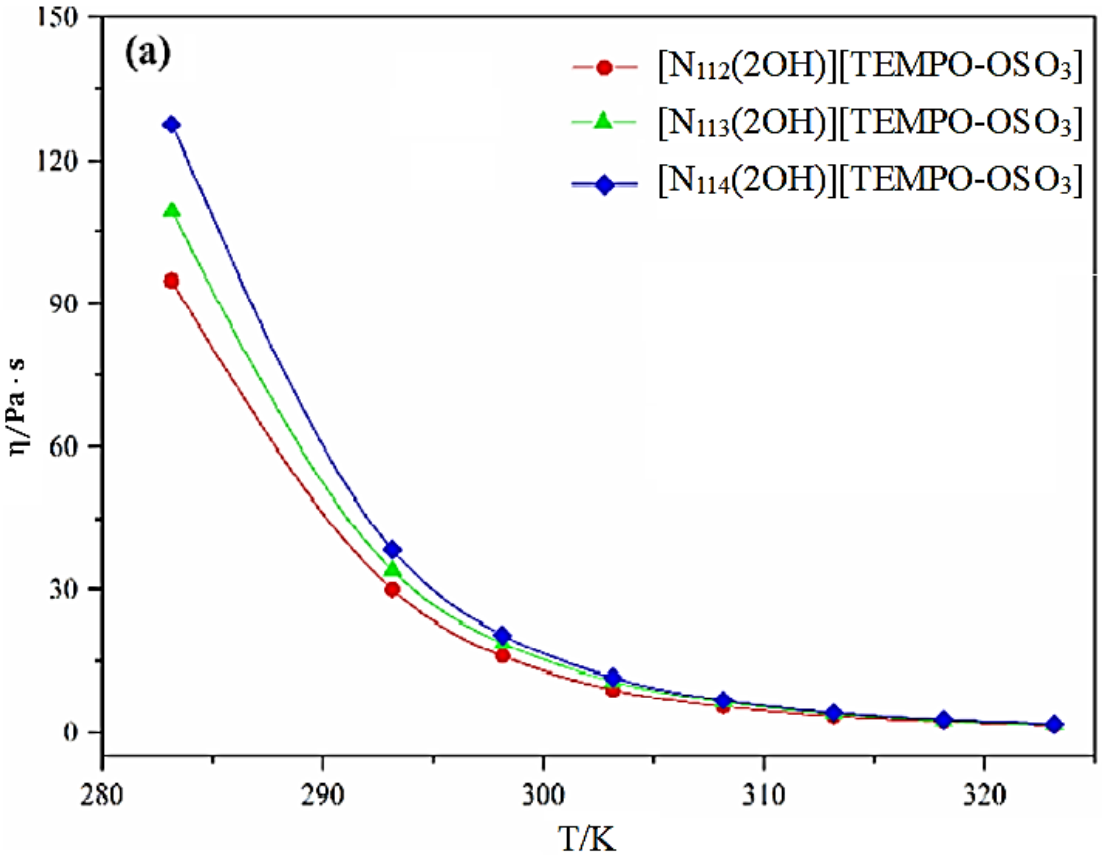

1 (a)

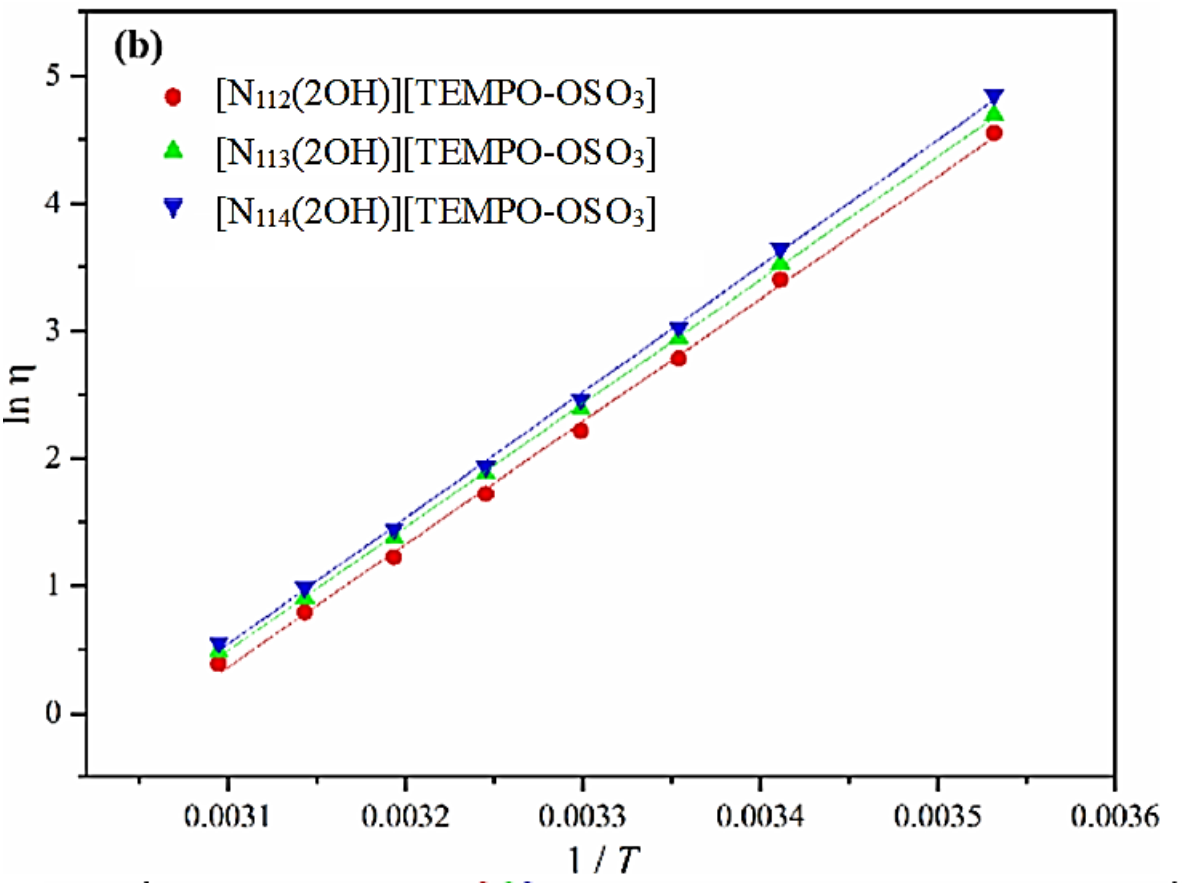

1(b)

Fig 1: (a) Dependence of viscosity of the MILs : $[N_{11n}(2OH)][TEMPO\text{-}OSO_3]$ on temperature (b) Plot of lnη against 1/T for three MILs.

TABLE 1: The viscosity of cholinium-based MILs at different temperature

Temperature (K)	Property	MIL 1	MIL 2	MIL 3
283.15	ν ×10² (m²/s)	8.02	9.31	11.12
	η (Pa·s)	94.75	109.50	127.40
293.15	ν ×10² (m²/s)	2.61	2.96	3.45
	η (Pa·s)	30.10	34.10	38.00
298.15	ν ×10² (m²/s)	1.43	1.69	1.84
	η (Pa·s)	16.25	18.85	20.70
303.15	ν ×10² (m²/s)	0.81	0.99	1.05
	η (Pa·s)	9.10	10.95	11.60
308.15	ν ×10² (m²/s)	0.5075	0.5942	0.6431
	η (Pa·s)	5.56	6.62	6.88
313.15	ν ×10² (m²/s)	0.3148	0.3732	0.4079
	η (Pa·s)	3.39	4.00	4.25
318.15	ν ×10² (m²/s)	0.2061	0.2378	0.2587
	η (Pa·s)	2.19	2.45	2.67
323.15	ν ×10² (m²/s)	0.1384	0.1583	0.1702
	η (Pa·s)	1.47	1.61	1.73

TABLE 2: The fitting parameters and correlation coefficient of $ln\eta$ against $1/T$ for five MILs.

MILs	Slope	Intercept	R^2
$[N_{112}(2OH)]$ [TEMPO-OSO_3]	9623.85	–29.47	0.99850
$[N_{113}(2OH)]$ [TEMPO-OSO_3]	9687.32	–29.54	0.99958
$[N_{114}(2OH)]$ [TEMPO-OSO_3]	9876.41	–30.07	0.99900

The viscosity data were correlated using the Vogel–Fulcher–Tamman (VFT), Litovitz, and Arrhenius equations, with the results compiled in Table 3. All three models provided excellent correlations, each yielding an R^2 value above 0.999. Notably, the standard deviation (SD) for the correlations followed the order: VFT equation < Arrhenius equation < Litovitz equation. The activation energy ($E\eta$) derived from the Arrhenius equation mirrored the viscosity trend: $[N_{114}(2OH)][TEMPO\text{-}OSO_3]$ >$[N_{113}(2OH)][TEMPO\text{-}OSO_3]$ >$[N_{112}(2OH)][TEMPO\text{-}OSO_3]$

TABLE 3: The fitting parameters of VFT equation Litovitz equation and Arrhenius equation (Viscosity correlated to temperature) for three MILs.

MILs	Equation	Parameters	Values	R^2	SD
$[N_{112}(2OH)][TEMPO\text{-}OSO_3]$	VFT	η_0 (Pa·s)	1.02×10^{-26}	0.99985	0.34210
		T_0 (K)	–258.103		
	Litovitz	A′	0.000478	0.99950	0.70512
		B (K^{-1})	34850.9		
	Arrhenius	$\eta\infty$ (Pa·s)	9.15×10^{-14}	0.99982	0.39275
		$E\eta$ (J)	1.33×10^{-19}		
		k	2.28×10^{9}		
$[N_{113}(2OH)][TEMPO\text{-}OSO_3]$	VFT	η_0 (Pa·s)	8.21×10^{-17}	0.99996	0.18510
		T_0 (K)	–62.113		
	Litovitz	A′	0.000561	0.99972	0.59880
		B (K^{-1})	14425.1		
	Arrhenius	$\eta\infty$ (Pa·s)	1.07×10^{-13}	0.99995	0.20400
		$E\eta$ (J)	1.34×10^{-19}		
		k	2.29×10^{9}		
$[N_{114}(2OH)][TEMPO\text{-}OSO_3]$	VFT	η_0 (Pa·s)	1.08×10^{-17}	0.99992	0.31240
		T_0 (K)	–68.430		
	Litovitz	A′	0.000439	0.99970	0.59977
		B (K^{-1})	15450.6		
	Arrhenius	$\eta\infty$ (Pa·s)	3.79×10^{-14}	0.99991	0.23011
		$E\eta$ (J)	1.39×10^{-19}		
		k	2.37×10^{9}		

To further understand the molecular basis of viscosity, the binding energy of the MIL anion and cation was calculated using Density Functional Theory (DFT). This computational approach employed Gaussian 16 software with the B3LYP hybrid functional and the 6-311G basis set. The binding energy (E_{bind}) was determined by subtracting the sum of individual ion energies (E_{cation}+ E_{anion}) from the optimized ion pair energy (E_{pair}): $E_{bind} = E_{pair} - (E_{cation} + E_{anion})$. The calculated binding energies for the three MIL systems are presented in Table 4. Interestingly, the viscosity values of the MILs were found to increase as the binding energy between the anion and cation decreased. This suggests that stronger cation–anion interactions promote the formation of more ordered microstructures, which, counter-intuitively, facilitates easier sliding or reorganization, thereby reducing internal friction and leading to lower macroscopic viscosity.

Table 4: Binding Energy Parameters for Three IL Systems

System	E_{pair} (kJ/mol)	E_{cation} (kJ/mol)	E_{anion} (kJ/mol)	E_{bind} (kJ/mol)
MIL1	−4,169,784.46	−1,065,946.05	−3,103,506.55	−331.86
MIL2	−4,272,986.63	−1,169,150.66	−3,103,506.55	−329.42
MIL3	−4,376,197.41	−1,272,374.63	−3,103,506.55	−316.23

3.3.1. Binodal Curve Analysis

The binodal curve provides crucial information on the concentrations of MILs and salts required to form aqueous two-phase systems (ATPSs), with a larger two-phase region indicating stronger phase formation ability. Binodal data for cholinium-based MIL-ATPSs were experimentally determined at various temperatures, utilizing five different salts (K_3PO_4,K_2HPO_4, K_2CO_3, $K_3C_6H_5O_7$, and $Na_3C_6H_5O_7$) known for their excellent salting-out efficiency and high water solubility. The experimental binodal data were theoretically correlated using the widely applied Merchuk equation $\left(w_1 = a \times exp(bw_2^{0.5} - cw_2^3)\right)$. The high correlation coefficients (R^2 > 0.99) and small standard deviations (SDs) confirm the accuracy of the experimental data and the suitability of the Merchuk equation for describing these MIL-ATPSs.

3.3.2. Effect of MIL Type on Binodal Curves

This section investigated the phase-forming ability of the three synthesized cholinium-based MILs using an inorganic salt (K_2HPO_4) and an organic salt ($K_3C_6H_5O_7$) [11]. The binodal data were correlated using the Merchuk equation, with parameters (a, b, c) and standard deviations (SD) provided in Table 5.

Table 5: Merchuk Equation Parameters for MILs + Salts + Water Systems at 298.15 K

System (MILs + Salt)	a	b	c	R^2	100SDa
$[N_{112}(2OH)][TEMPO\text{-}OSO_3]+ K_2HPO_4$	0.9982	−3.3756	50.384	0.9984	0.4156
$[N_{113}(2OH)][TEMPO\text{-}OSO_3]+ K_2HPO_4$	1.4381	−3.9781	62.963	0.9988	0.5501
$[N_{114}(2OH)][TEMPO\text{-}OSO_3]+ K_2HPO_4$	1.3670	−4.4140	64.380	0.9972	0.6123
$[N_{112}(2OH)][TEMPO\text{-}OSO_3]+ K_3C_6H_5O_7$	1.4053	−3.1993	17.3754	0.9924	1.2354
$[N_{113}(2OH)][TEMPO\text{-}OSO_3] + K_3C_6H_5O_7$	0.9864	−1.8564	50.805	0.9979	0.7673
$[N_{114}(2OH)][TEMPO\text{-}OSO_3]+ K_3C_6H_5O_7$	1.0962	−2.6682	36.465	0.9989	0.5266

As illustrated in Fig. 4$[N_{114}(2OH)][TEMPO\text{-}OSO_3]$ consistently exhibited the widest biphasic region, indicating its superior phase-forming ability. The salting-out effect is identified as the primary driving force for phase separation. At high salt concentrations, the phase separation ability of the MILs increased with the elongation of the cationic carbon chain, aligning with trends observed for imidazolium ILs [12-14]. However, at low salt concentrations (high MIL content), irregular changes in the phase diagram were observed, influenced by the higher viscosity of the MILs, which can hinder aggregation processes.

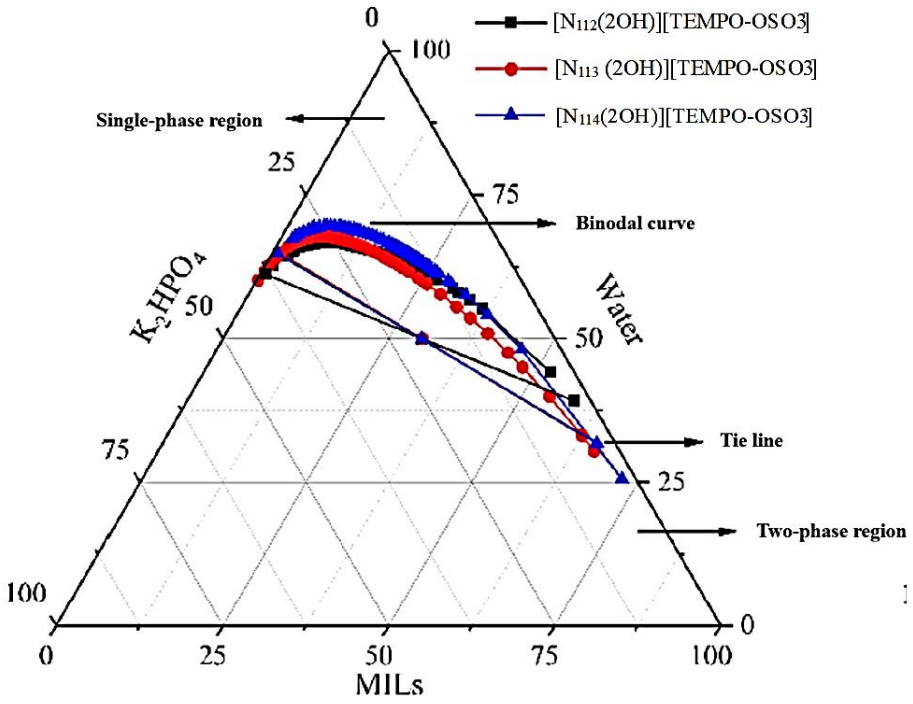

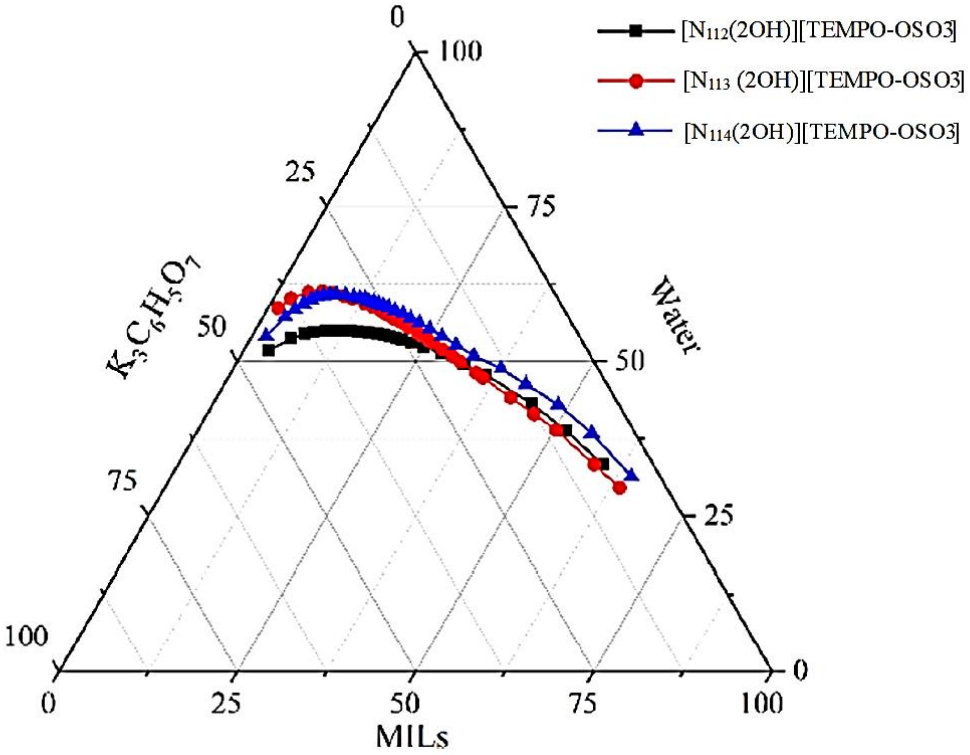

Figure 4: Effect of different MILs on binodal curves

Furthermore, the hydrophilic and hydrophobic properties of the MILs significantly affected their phase-forming ability [13]. Increased hydrophobicity, often linked to longer carbon chains, generally enhances the phase-forming capacity of ILs. The formation of MIL-ATPSs is a competitive process for water molecules between the MIL and the salt. The elongation of the cation carbon chain promotes water transfer from the top to the bottom phase, resulting in a higher MIL concentration and a lower salt requirement for ATPS formation. Thus, hydrophobic interaction is a major contributor to the MILs' phase-formation ability.

3.3.3. Effect of Salt Type on Binodal Curves

This study investigated the influence of five different salts (three inorganic: K_3PO_4, K_2HPO_4, K_2CO_3; and two organic: $K_3C_6H_5O_7$, $Na_3C_6H_5O_7$) on the formation of ATPSs with the three MILs at 298.15 K. Fitting parameters provided in Table 6. The calculated binodal curves for all five salts are presented in Fig. 2, demonstrating a consistent effect across all MIL types and satisfactory phase separation.

Table6: Merchuk Equation Parameters for MILs + Different Salts + Water Systems at 298.15 K

MIL System	Salt	a	B	c	R^2	100SD
$[N_{112}(2OH)][TEMPO\text{-}OSO_3]$	K_3PO_4	0.6662	−2.2664	102.960	0.9997	0.1568
	K_2HPO_4	0.9982	−3.3756	50.384	0.9984	0.4156
	K_2CO_3	1.0232	−2.8751	53.4563	0.9989	0.4421
	$K_3C_6H_5O_7$	1.4053	−3.1993	17.3754	0.9924	1.2354
	$Na_3C_6H_5O_7$	1.3270	−3.6943	30.2618	0.9996	0.1755
$[N_{113}(2OH)][TEMPO\text{-}OSO_3]$	K_3PO_4	1.1436	−3.3399	133.210	0.9979	0.6381
	K_2HPO_4	1.4381	−3.9781	62.963	0.9988	0.5501
	K_2CO_3	1.3238	−3.0410	77.022	0.9993	0.3898
	$K_3C_6H_5O_7$	0.9864	−1.8564	50.805	0.9979	0.7673
	$Na_3C_6H_5O_7$	1.5073	−3.5798	54.328	0.9965	0.9508
$[N_{114}(2OH)][TEMPO\text{-}OSO_3]$	K_3PO_4	1.0693	−3.7740	105.270	0.9966	0.7734
	K_2HPO_4	1.3670	−4.4140	64.380	0.9972	0.6123
	K_2CO_3	1.2729	−3.6623	76.780	0.9987	0.5341
	$K_3C_6H_5O_7$	1.0962	−2.6682	36.465	0.9989	0.5266
	$Na_3C_6H_5O_7$	1.2370	−3.5697	48.317	0.9979	0.7218

The salting-out ability of the investigated salts followed the order: K_3PO_4> K_2HPO_4> K_2CO_3> $Na_3C_6H_5O_7$> $K_3C_6H_5O_7$. K_3PO_4 exhibited a significantly wider binodal curve range, indicating superior salting-out ability, likely due to its higher water solubility, which efficiently excludes the MIL from the solution [15-17].

For anions, the salting-out ability followed the order: $PO4^{3-} > HPO4^{2-} > CO_3^{2-} > C_6H_5O_7^{3-}$, demonstrating that higher charge density in inorganic anions corresponds to a stronger salting-out effect.

Journal of

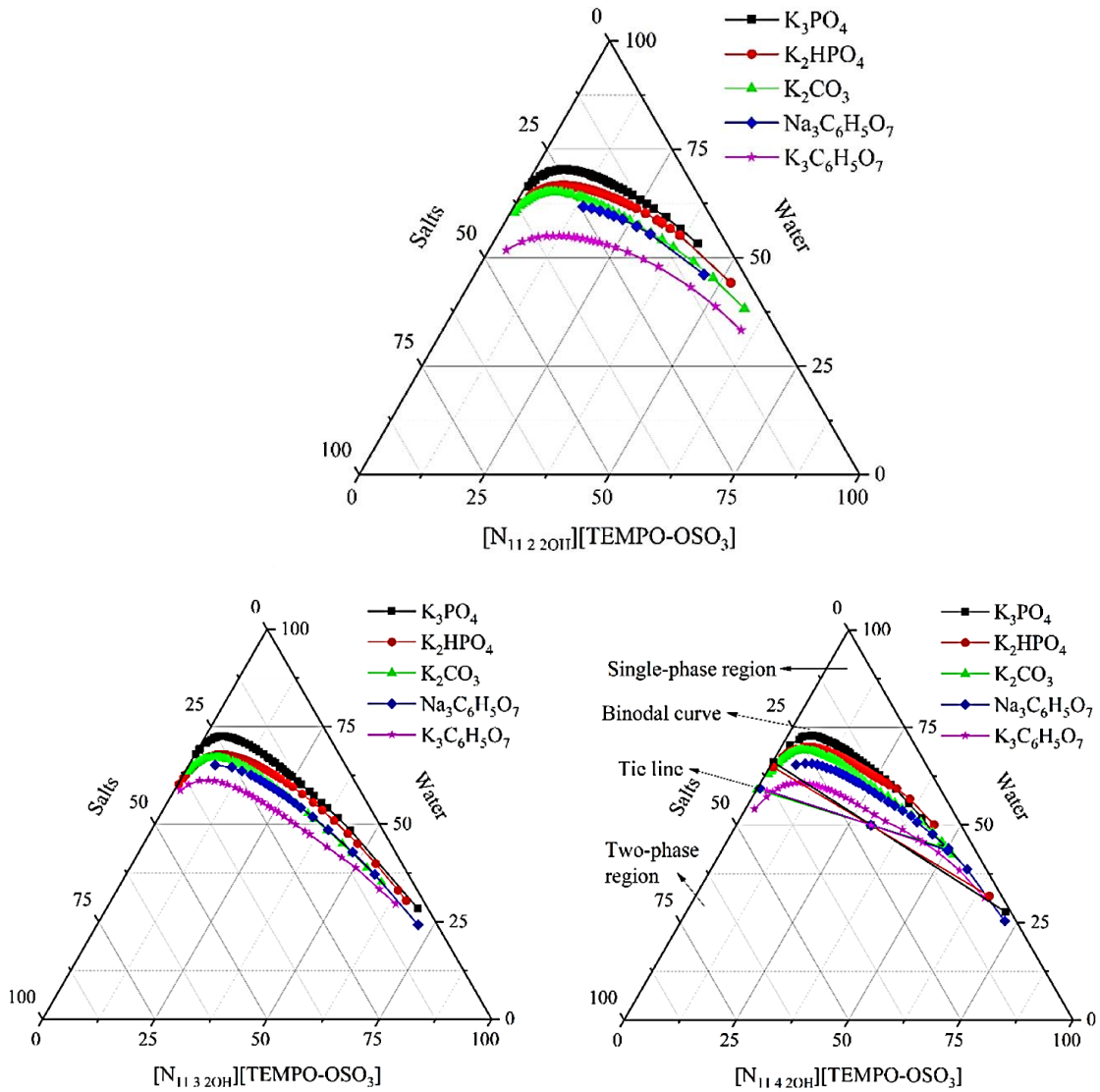

Figure 2: Effect of salts on binodal curves (a) $[N_{112}(2OH)][TEMPO\text{-}OSO_3]$ (b) $[N_{113}(2OH)][TEMPO\text{-}OSO_3]$ (c) $[N_{114}(2OH)][TEMPO\text{-}OSO_3]$.

Crucially, the salting-out abilities of the inorganic salt ions correlated closely with their Gibbs free energy of hydration ($\Delta_{hyd}G$) and entropy of hydration ($\Delta_{hyd}S$) [38–40], as shown in Table 7. The order of the absolute values of $\Delta_{hyd}G$ and $\Delta_{hyd}S$ for anions precisely matched their salting-out order. Similarly, for citrate-based salts, the cation salting-out ability followed $Na^+ > K^+$, also consistent with their respective $\Delta_{hyd}G$ and $\Delta_{hyd}S$ values listed in Table 7. In conclusion, the impact of salts on salting-out ability adhered to the Hofmeister series, which is in agreement with findings for imidazolium-based ILs [18-20].

Table 7: Values of ΔhydG and ΔhydS for Common Anions and Cations of Salts

Salt Ion	**PO_4^{3-}**	**HPO_4^{2-}**	**CO_3^{2-}**	**Na^+**	**K^+**
ΔhydG (kJ/mol)	−2765	−1789	−1315	−365	−295
ΔhydS (J/K·mol)	−421	−272	−245	−111	−74

3.4. Mechanism of Phase Separation

The phase separation mechanism in MIL-ATPSs is primarily governed by the salting-out effect, driven by the competition for water molecules between the MIL and the salt. The hydrophobicity of the MILs significantly influences phase formation; a longer carbon chain in the cationic structure (e.g., ($[N_{114}(2OH)][TEMPO\text{-}OSO_3]$) enhances hydrophobicity, leading to stronger phase formation ability. MIL

viscosity, which depends on inter-ionic interactions (electrostatic, van der Waals, hydrogen bonding), also plays a role, where stronger internal interactions are conducive to phase separation [21-25]. Furthermore, the hydrogen-bond alkalinity of these cholinium-based MILs, tunable by cation carbon chain length, affects phase separation: weaker alkalinity (longer carbon chain) reduces MIL-water hydrogen bonding, promoting phase separation.

Salt properties are equally critical. Kosmotropic ions (e.g., $SO4^{2-}$, $HPO4^{2-}$, $CO3^{2-}$, Na^{+}, K^{+}) induce a more ordered water arrangement, influencing phase formation. The salting-out ability of these ions directly correlates with their Gibbs free energy of hydration ($\Delta_{hyd}G$) and entropy of hydration ($\Delta_{hyd}S$), where lower values indicate stronger phase formation. Lastly, temperature's effect on phase behavior shows that higher temperatures promote a larger biphasic area, signifying an endothermic and entropically driven phase separation process, confirming the MIL-ATPS's low critical solution temperature (LCST) phase transition behavior [26-28].

IV. Conclusions

This study successfully synthesized and characterized three cholinium-based magnetic ionic liquids (MILs) and demonstrated their effectiveness in forming magnetically responsive aqueous two-phase systems (ATPSs). We thoroughly investigated the phase behavior of these MIL-ATPSs, precisely fitting binodal data with the Merchuk equation. Our findings reveal that the MIL structure, temperature, and salt type are crucial factors profoundly influencing phase behavior. Specifically, MIL structural features and viscosity significantly impact phase formation. The salting-out effect was identified as the primary driving force for phase separation, showing a clear correlation with the hydration thermodynamics ($\Delta_{hyd}G$ and $\Delta_{hyd}S$) of the salts. These comprehensive experimental and theoretical insights are invaluable for the continued development and rational design of advanced, responsive separation technologies.

References

[1] M. Singla, N. Sit, Theoretical aspects and applications of aqueous two-phase systems, ChemBioEng Rev. 10 (1) (2023) 65–80, https://doi.org/10.1002/ cben.202200026.
[2] P.-Å. Albertsson, Partition of cell particles and macromolecules in polymer two- phase systems, Adv. Protein Chem. 24 (1970) 309–341, https://doi.org/10.1016/ S0065-3233(08)60244-2.
[3] Y. Huang, Y. Liu, Y. Ruan, J. Gong, L. Kong, M. Su, W. Han, M. Yang, D. Chen, A sulfonated ligand-aqueous two-phase system for selective extraction of thorium from mining wastewater: process optimization, structural characterization and mechanism exploration, J. Mol. Liq. 384 (2023) 122223, https://doi.org/10.1016/ j.molliq.2023.122223.
[4] C. A. Suarez Ruiz, J. Kwaijtaal, O. C. Peinado, C. van den Berg, R. H. Wijffels, M. H. M. Eppink, Multistep fractionation of microalgal biomolecules using selective aqueous two-phase systems, ACS Sust. Chem. Eng. 8 (6) (2020) 2441–2452, doi: 10.1021/acssuschemeng.9b06379.
[5] T. Ahmed, C. Yamanishi, T. Kojima, S. Takayama, Aqueous two-phase systems and microfluidics for microscale assays and analytical measurements, Annu. Rev. Anal. Chem. 14 (2021) 231–255, https://doi.org/10.1146/annurev-anchem-091520- 101759.
[6] K.E. Gutowski, G.A. Broker, H.D. Willauer, J.G. Huddleston, R.P. Swatloski, J. D. Holbrey, R.D. Rogers, Controlling the aqueous miscibility of ionic liquids: aqueous biphasic systems of water-miscible ionic liquids and water-structuring salts for recycle, metathesis, and separations, J. Am. Chem. Soc. 125 (22) (2003) 6632–6633, https://doi.org/10.1021/ja035180.
[7] J.C. Merchuk, B.A. Andrews, J.A. Asenjo, Aqueous two-phase systems for protein separation: studies on phase inversion, J. Chromatogr. B 711 (1–2) (1998) 285–293, https://doi.org/10.1016/S0378-4347(97)00594-X.
[8] S.P. Ventura, C.M. Neves, M.G. Freire, I.M. Marrucho, J. Oliveira, J.A. Coutinho, Evaluation of anion influence on the formation and extraction capacity of ionic- liquid-based aqueous biphasic systems, J. Phys. Chem. B 113 (27) (2009) 9304–9310, https://doi.org/10.1021/jp903286d.
[9] M.T. Zafarani-Moattar, S. Tolouei, Liquid-liquid equilibria of aqueous two-phase systems containing polyethylene glycol 4000 and di-potassium tartrate, potassium sodium tartrate, or di-potassium oxalate: experiment and correlation, Calphad 32 (4) (2008) 655–660, https://doi.org/10.1016/j.calphad.2008.09.006.
[10] Y. Wang, S. Hu, J. Han, Y. Yan, Measurement and correlation of phase diagram data for several hydrophilic alcohol+citrate aqueous two-phase systems at 298.15 K, J. Chem. Eng. Data 55 (11) (2010) 4574-4579, doi: 10.1021/je9007348.
[11] Y. Shu, M. Gao, X. Wang, R. Song, J. Lu, X. Chen, Separation of curcuminoids using ionic liquid based aqueous two-phase system coupled with in situ dispersive liquid- liquid microextraction, Talanta 149 (2016) 6–12, https://doi.org/10.1016/j. talanta.2015.11.009.
[12] Y. Wang, X. Xu, Y. Yan, J. Han, Z. Zhang, Phase behavior for the [Bmim]BF4 aqueous two-phase systems containing ammonium sulfate/sodium carbonate salts at different temperatures: experimental and correlation, Thermochim. Acta 501 (1) (2010) 112–118, https://doi.org/10.1016/j.tca.2010.01.020.
[13] S. Li, C. He, H. Liu, K. Li, F. Liu, Ionic liquid-based aqueous two-phase system, a sample pretreatment procedure prior to high-performance liquid chromatography of opium alkaloids, J. Chromatogr. B 826 (1–2) (2005) 58–62, https://doi.org/ 10.1016/j.jchromb.2005.08.005.
[14] M.T. Zafarani-Moattar, V. Hosseinpour-Hashemi, Effect of temperature on the aqueous two-phase system containing poly (ethylene glycol) dimethyl ether 2000 and dipotassium oxalate, J. Chem. Eng. Data 57 (2) (2012) 532–540, https://doi. org/10.1021/je201101e.
[15] J. Han, C. Yu, Y. Wang, X. Xie, Y. Yan, G. Yin, W. Guan, Liquid-liquid equilibria of ionic liquid 1-butyl-3-methylimidazolium tetrafluoroborate and sodium citrate/ tartrate/acetate aqueous two-phase systems at 298.15K: experiment and correlation, Fluid Phase Equilibr. 295 (1) (2010) 98–103, doi: 10.1016/j. fluid.2010.03.044.
[16] Y. Li, M. Zhang, Q. Liu, H. Su, Phase behaviour for aqueous two-phase systems containing the ionic liquid 1-butylpyridinium tetrafluoroborate/1-butyl-4- methylpyridinium tetrafluoroborate and organic salts (sodium tartrate/ammonium citrate/trisodium citrate) at different temperatures, J. Chem. Thermodyn. 66 (2013) 80–87, https://doi.org/10.1016/j.jct.2013.06.011.
[17] C. Wu, J. Wang, H. Wang, Y. Pei, Z. Li, Effect of anionic structure on the phase formation and hydrophobicity of amino acid ionic liquids aqueous two-phase systems, J. Chromatogr. A 1218 (48) (2011) 8587–8593, https://doi.org/10.1016/ j.chroma.2011.10.003.

[18] T. Yao, H. Zang, S. Yao, X. Dai, H. Song, Measurement and correlation of phase equilibria in aqueous two-phase systems containing functionalized magnetic ionic liquids and potassium phosphate at different temperatures, J. Mol. Liq. 263 (2018) 72–80, https://doi.org/10.1016/j.molliq.2018.04.131.
[19] L. Das, F. Rubbi, K. Habib, N. Aslfattahi, R. Saidur, B.B. Saha, S. Algarni, K. Irshad, T. Alqahtani, State-of-the-art ionic liquid &ionanofluids incorporated with advanced nanomaterials for solar energy applications, J. Mol. Liq. 336 (2021) 116563, https://doi.org/10.1016/j.molliq.2021.116563.
[20] A.M. Curreri, S. Mitragotri, E.E. Tanner, Recent advances in ionic liquids in biomedicine, Adv. Sci. 8 (17) (2021) 2004819, https://doi.org/10.1002/ advs.202004819.
[21] L. Nie, Z. Zheng, M. Lu, S. Yao, D. Guo, Phase behavior of ionic liquid-based aqueous two-phase systems, Int. J. Mol. Sci. 23 (20) (2022) 12706, https://doi.org/ 10.3390/ijms232012706.
[22]H.-F. Jin, Y. Shi, M.-Z. Shi, J. Cao, L.-H. Ye, Ionic liquid-assisted aqueous two-phase system for the enrichment of multiple monosaccharides from jujube, Ind. Crop. Prod. 204 (2023) 117392, https://doi.org/10.1016/j.indcrop.2023.117392.
[23]Y. Li, X. Li, X. Wang, J. Xue, R. Zhang, Y. Ding, X. Chu, J. Su, Study on extraction and purification of acanthopanaxsenticosus polyphenols by an ionic liquid-assisted aqueous two-phase system, Molecules 28 (17) (2023) 6383, https://doi.org/ 10.3390/molecules28176383.
[24]F.S. Buarque, A. Carniel, B.D. Ribeiro, M.A.Z. Coelho, Selective enzymes separation from the fermentation broth of Yarrowialipolytica using aqueous two-phase system based on quaternary ammonium compounds, Sep. Purif. Technol. 324 (2023) 124539, https://doi.org/10.1016/j.seppur.2023.124539.
[25] X. Feng, W. Zhang, T. Zhang, S. Yao, Systematic investigation for extraction and separation of polyphenols in tea leaves by magnetic ionic liquids, J. Sci. Food Agr. 98 (12) (2018) 4550–4560, https://doi.org/10.1002/jsfa.8983.
[26]L.-R. Nie, S. Yao, B. Dong, X.-L. Li, H. Song, Synthesis, characterization and physical properties of novel cholinium-based organic magnetic ionic liquids, J. Mol. Liq. 240 (2017) 152–161, https://doi.org/10.1016/j.molliq.2017.05.044.
[27]C. Zhu, Z. Wang, R. Ma, W. Wu, M. Dong, X. Chen, Y. Du, D. Tang, S. Ji, Selective enrichment of licorice triterpenoid saponins from complicated samples by magnetic poly (ionic liquid)-functionalized metal-organic framework, Lwt-Food Sci. Technol. 185 (2023) 115143, https://doi.org/10.1016/j.lwt.2023.115143.
[28] R. Goutham, P. Rohit, S.S. Vigneshwar, A. Swetha, J. Arun, K.P. Gopinath, A. Pugazhendhi, Ionic liquids in wastewater treatment: a review on pollutant removal and degradation, recovery of ionic liquids, economics and future perspectives, J. Mol. Liq. 349 (2022) 118150, https://doi.org/10.1016/j. molliq.2021.118150.